Preprint typeset in JINST style - HYPER VERSION

Characteristics of saturation spectroscopy at the Balmer-α line of atomic hydrogen in a linear magnetized plasma source

Renge Asakawa[a], Motoshi Goto[b], Nader Sadeghi[c], and Koichi Sasaki[d]*

[a] *Department of Electrical Engineering and Computer Science, Nagoya University, Furo-cho, Chikusa-ku, Nagoya 464-8603, Japan*
[b] *National Institute for Fusion Science, 322-6 Oroshi-cho, Toki 509-5292, Japan*
[c] *LIPhy, Universite Joseph Fourier & CNRS, Grenoble, France*
[d] *Division of Quantum Science and Engineering, Hokkaido University, Kita 13, Nishi 8, Kita-ku, Sapporo 060-8628, Japan*
E-mail: sasaki@qe.eng.hokudai.ac.jp

ABSTRACT: We adopted saturation spectroscopy for observing a Doppler-free spectrum of the Balmer-α line of atomic hydrogen in a linear magnetized plasma source. The spectrum was composed of a broadband offset and many peaks which were assigned as fine-structure components of the Balmer-α line with Zeeman splitting. We examined the amplitudes of the offset and line components as functions of the pump laser power and the discharge gas pressure. The saturation parameter or the amplitude of the saturation spectrum was discussed by referring to the theory of saturation spectroscopy. In addition, the physical origin of the broadband offset component was speculated on the basis of the pressure dependence of the saturation spectrum.

KEYWORDS: Saturation spectroscopy; Balmer-α line of atomic hydrogen; Saturation parameter; Plasma diagnostics.

*Corresponding author.

Contents

1. Introduction

Laser absorption spectroscopy has a much finer resolution than optical emission spectroscopy, and is widely used for investigating the velocity distribution functions of various species in plasmas by measuring Doppler-broadened spectra of their transition lines [1–6]. On the other hand, studies of the particle balance in Large Helical Device (LHD) at the National Institute for Fusion Science (NIFS) need a spectral resolution finer than the Doppler broadening. A required information for understanding the particle balance is the location of ionization ($H + e \rightarrow H^+ + e + e$). The location of ionization is expected to be almost the same as the location of excitation ($H + e \rightarrow H^* + e$) in the LHD plasma [7]. In principle, the location of excitation is known by measuring the spectrum of the Balmer-α line of atomic hydrogen with Zeeman splitting, since the spatial distribution of the magnetic field strength is known in LHD and the spectrum with Zeeman splitting is a fingerprint of the magnetic field strength. However, because of a high temperature of atomic hydrogen in LHD, the details of Zeeman splitting are masked by the Doppler broadening [8, 9]. Under the aforementioned background, in this work, we developed a system of saturation spectroscopy at the Balmer-α line of atomic hydrogen.

Saturation spectroscopy has a Doppler-free resolution, and is widely used in the field of fundamental spectroscopy, where researchers are interested in ultrafine determinations of the wavelengths of various transition lines [10]. Although plasmas are frequently used in fundamental

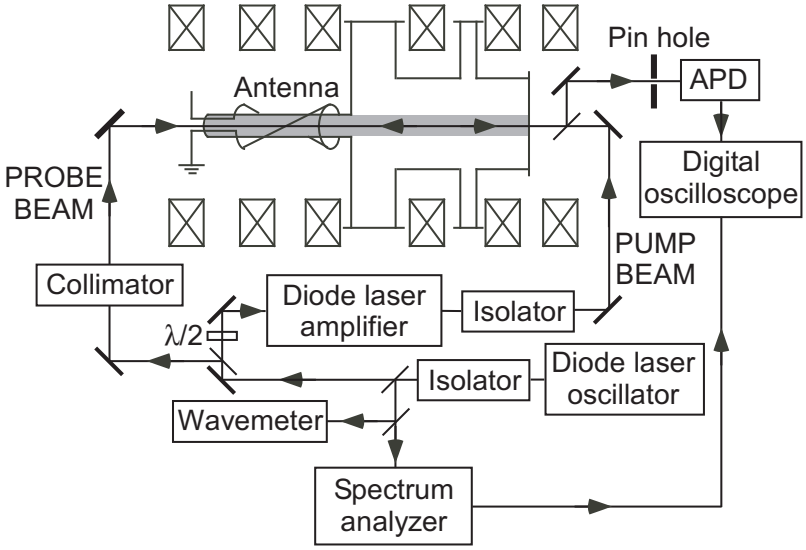

Figure 1. Experimental apparatus.

spectroscopy as a method to obtain excited states of various species, the relationship between the spectral characteristics and plasma parameters is not interested so much. However, when we develop a system of saturation spectroscopy with the intention of applying it to plasma diagnostics, it is necessary to investigate its spectral characteristics as functions of plasma parameters. The shift and the broadening of fine-structure components of the hydrogen Balmer-α line were investigated by Weber and coworkers in unmagnified hollow cathode arc discharges approximately thirty years ago [11–13], where they used saturation-polarization spectroscopy to obtain a Doppler-free resolution. In this work, we examined characteristics of simple saturation spectroscopy in a magnetized linear plasma source. The saturated absorption spectra were measured as functions of the pump laser power and the discharge gas pressure. A novelty of this work is our interest in collisional effects in plasmas on characteristics of saturation spectroscopy at the Balmer-α line of atomic hydrogen.

2. Experiment

2.1 Plasma source

The experimental apparatus is illustrated in figure 1. The plasma source was a linear machine with a uniform magnetic field of 350 G along the axis. The helical antenna wound around the quartz glass tube was connected to an rf power supply at 13.56MHz via a matching circuit. The diameter of the glass tube was 1.6 cm, and a plasma column with the same diameter as the glass tube was confined radially by the external magnetic field. The lengths of both the glass tube and the diffusion chamber were 30 cm. The vacuum chamber was evacuated using a turbomolecular pump below a background pressure of 5×10^{-6} Torr.

This plasma source had two discharge modes [14]. One was “the low-density mode”, which was realized at a low rf power. The range of the plasma density in the low-density mode was on the

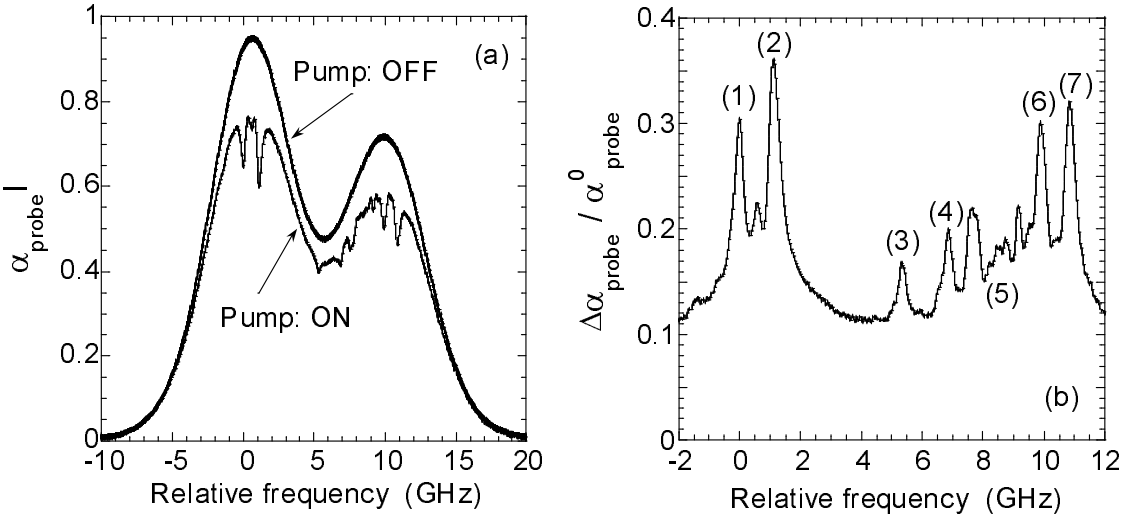

Figure 2. Spectra of simple laser absorption spectroscopy and saturation spectroscopy, observed in a low-density mode discharge. The two curves shown in (a) represents the absorbance spectra of the probe laser beam with and without the pump laser beam. (b) was obtained by dividing the difference between the two curves shown in (a) by the absorbance spectrum without the pump laser beam.

order of 10^{11} cm^{-3}. The other was "the high-density mode". The plasma density increased by a factor of ~ 100 at an rf power (called "a helicon jump"), and the range of the plasma density in the high-density mode was on the order of 10^{13} cm^{-3}. In this study, we mainly used low-density mode discharges employing pure H_2 gas. High-density mode discharges were used in some experiments, where we used the mixture of H_2 and Ar since the absorption of the probe laser beam was close to 100% when we used pure H_2 for high-density mode discharges.

2.2 System for saturation spectroscopy

The light source for saturation spectroscopy was an oscillator-amplifier system of diode lasers, which yielded tunable, single-mode, cw radiation with a power of approximately 200 mW. The wavelength of the master oscillator (New Focus, Vortex II) was scanned for a range of 50 GHz within a period of 5 ms. The power and the linewidth of the master oscillator were approximately 15 mW and less than 1 MHz, respectively. A part of the master oscillator beam (< 1 mW) was picked up using a beam splitter and was used as the probe beam. A collimator was used for avoiding the divergence of the probe beam. In addition, a part of the master oscillator beam was picked up to measure the rough wavelength and the frequency scan using a wavemeter and a Fabry-Pérot spectrum analyzer, respectively. The other part of the master oscillator beam was injected into a diode laser amplifier (TOPTICA, BoosTA) to obtain the intense pump beam. A half-wavelength plate was inserted between the oscillator and the amplifier to adjust the direction of polarization. The pump laser power was varied by changing the current of the diode laser amplifier.

The probe and pump beams were launched into the plasma source from the counter axial directions, and they were overlapped carefully. Therefore, the present experimental configuration was sensitive to the σ transitions between energy levels with Zeeman splitting. A beam splitter

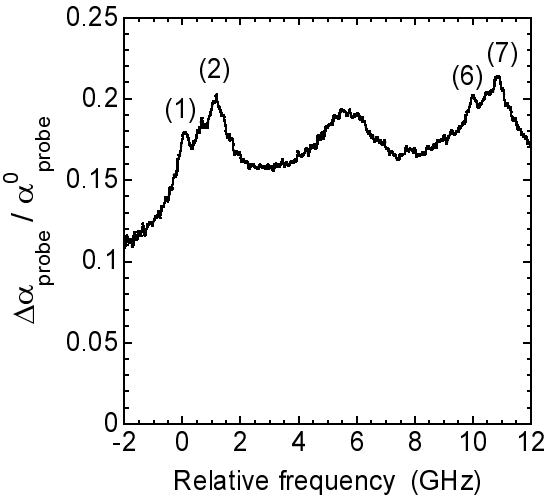

Figure 3. Similar spectrum to figure 2b observed in a high-density mode discharge.

was used for detecting the transmitted probe beam using an avalanche photo diode. A pin hole transmitted the probe beam, while it eliminated the optical emission from the plasma efficiently. The electrical signal from the avalanche photo diode was recorded using a digital oscilloscope, together with the signal from the spectrum analyzer. The time axis of the digital oscilloscope was converted into the relative frequency of the master oscillator by referring to the signal from the spectrum analyzer.

3. Results

3.1 Spectrum of saturation spectroscopy

Spectra of the probe beam transmitted through a plasma are shown in figure 2a, which was observed with and without the pump laser beam. The origin of the relative frequency axis corresponds to a wavelength of 656.285 nm. The vertical axis shows the absorbance, which is the product between the absorption coefficient for the probe beam ($\alpha_{\rm probe}$) and the absorption length (ℓ), and is obtained from the intensities of the incident (I_0) and transmitted ($I_{\rm t}$) probe laser beams using the Lambert-Beer law $\alpha\ell = -\ln(I_{\rm t}/I_0)$. The plasma was produced at an rf power of 700 W in pure H_2 gas at a pressure of 50 mTorr, which was a typical condition for the low-density mode discharge. The pump laser power in front of the optical window for launching the pump beam into the plasma was 146 mW. When the pump laser beam was switched off, we observed a smooth spectrum with two broad peaks, as shown in figure 2a, which was understood by the overlaps of many Doppler-broadened fine-structure components of the Balmer-α line [3]. On the other hand, when the pump beam was switched on, we observed many dips in the spectrum of the probe beam, as shown in figure 2a.

Figure 2b shows a saturation spectrum, which was obtained by dividing the difference between the two spectra ($\Delta\alpha_{\rm probe}$) shown in figure 2a by the spectrum without the pump laser beam ($\alpha^0_{\rm probe}$). We observed many peaks with high spectral resolutions. The assignments of the peaks labeled in figure 2b will be discussed in the next section. A similar result to figure 2b is shown in figure 3,

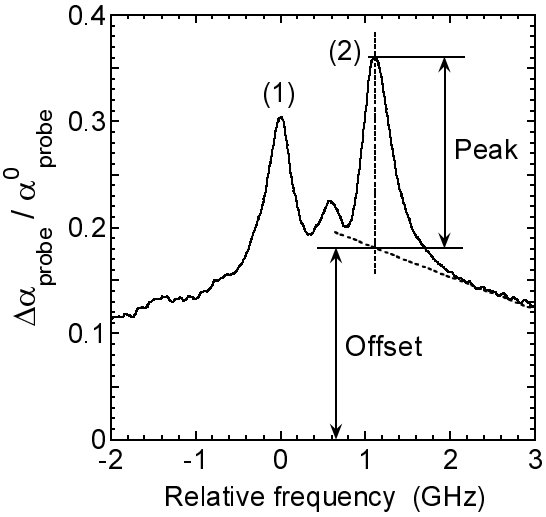

Figure 4. Definitions of the amplitudes of the peak and offset components.

which was observed in a high-density mode discharge. The rf power was 2 kW, and the discharge gas was the mixture of H_2 and Ar at partial pressures of 4.5 and 18 mTorr, respectively. The dips induced by the pump laser beam were also observed in the high-density mode discharge. The dip spectrum shown in figure 3 has smaller amplitudes and broader widths than the dip spectrum shown in figure 2b.

3.2 Dependence of the saturation spectrum on the pump laser power

Figure 4 shows an expanded spectrum of a part of figure 2b. As shown in the figure, the saturation spectrum was composed of narrow peak and broadband offset components. We defined the amplitudes ($\Delta\alpha_{\rm probe}/\alpha^0_{\rm probe}$) of the narrow peak and the broadband offset as illustrated in figure 4 for the case of the peak labeled with (2) in figure 2b. Figure 5 shows the amplitudes of the peak and offset components as a function of the pump laser power. This result was obtained in a low-density mode discharge. As shown in figure 5a, the amplitude of the peak component was roughly proportional to the pump laser power in the low-power regime ($<$ 20 mW), while we observed a saturation of the increase in the amplitude of the peak component at pump laser powers higher than 20 mW. The amplitude of the offset component was also roughly proportional to the pump laser power, as shown in figure 5b. A weak saturation of the increase in the amplitude of the offset component was also observed in the high-power regime ($>$ 70 mW).

3.3 Dependence of the saturation spectrum on the gas pressure

From the viewpoint of application to plasma diagnostics, it is important to examine the dependence of the saturation spectrum on plasma parameters. Here, we measured the amplitudes of the peak and offset components for the line labeled with (2) in figure 2b as a function of the discharge gas pressure. The rf power was 750 W (low-density mode discharges), and the pump laser power was 100 mW. As shown in figure 6a, the amplitude of the peak component decreased with the gas

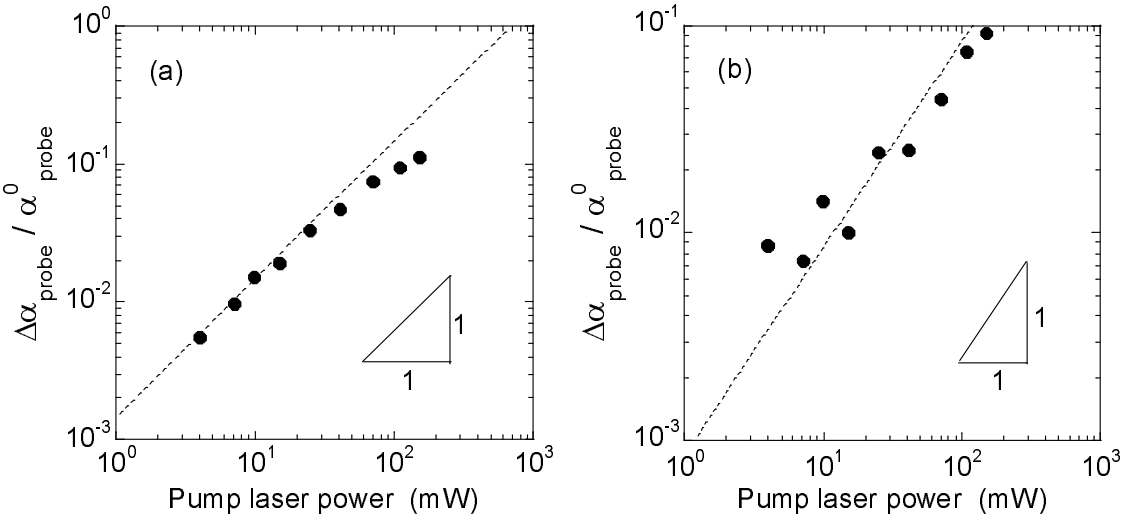

Figure 5. Amplitudes of the (a) peak and (b) offset components as a function of the pump laser power.

pressure, while the amplitude of the offset component increased with the gas pressure as shown in figure 6b. This means that the signal-to-noise ratio of the saturation spectrum becomes low in a discharge at a high gas pressure.

4. Discussion

4.1 Theory of saturation spectroscopy

According to the theory of saturation spectroscopy [15], the shape of the saturation spectrum for a transition line is given by

$$\frac{\Delta\alpha_{\rm probe}}{\alpha^0_{\rm probe}} = \frac{S}{2}\frac{(\gamma_{\rm s}/2)^2}{(\omega-\omega_0)^2+(\Gamma^*_{\rm s}/2)^2}, \tag{4.1}$$

where S is called saturation parameter, $\alpha^0_{\rm probe}$ is the absorption coefficient for the probe laser beam when the pump laser beam is switched off, $\Delta\alpha_{\rm probe}$ is the difference in the absorption coefficients with and without the pump laser beam, $\omega-\omega_0$ denotes the deviation of the angular frequency from the center of the transition line, $\gamma_{\rm s}=\gamma\sqrt{1+S}$ with γ being the homogeneous width of the transition line, and $\Gamma^*_{\rm s}=(\gamma+\gamma_{\rm s})/2$. Equation (4.1) is accurate when $S \ll 1$. The saturation parameter S is given by

$$S = B_{23}\rho\left(\frac{1}{R_2}+\frac{1}{R_3}\right), \tag{4.2}$$

where ρ is the spectral power density of the pump laser beam, R_2 and R_3 are the relaxation frequencies of the lower ($n=2$) and upper ($n=3$) energy states, respectively, and B_{23} is Einstein's B coefficient for the transition line. The absorption coefficient for the pump beam is given as a function of the saturation parameter such that

$$\alpha_{\rm pump} = \frac{\alpha^0_{\rm pump}}{1+S}, \tag{4.3}$$

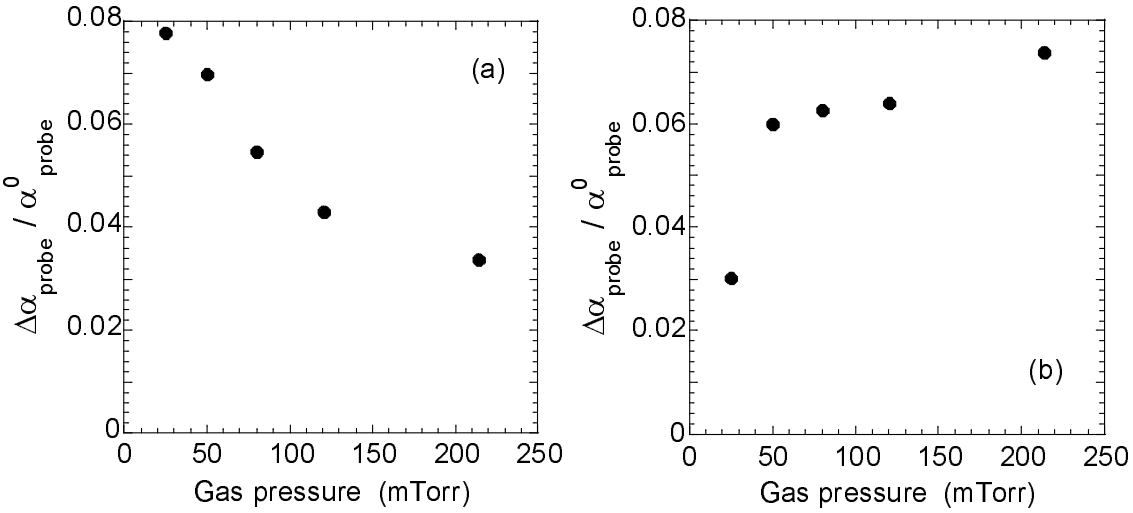

Figure 6. Amplitudes of the (a) peak and (b) offset components as a function of the discharge gas pressure.

where $\alpha^0_{\rm pump}$ is the absorption coefficient for the pump beam when the pump laser power is so weak that the saturation of absorption is negligible ($\alpha^0_{\rm probe} = \alpha^0_{\rm pump}$).

4.2 Assignment of peaks

Since the Balmer-α line is composed of many fine-structure transitions, the saturation spectrum has many lines, each of which has a line shape expressed by equation (4.1). The Zeeman-split line components were calculated using a method based on the perturbation theory [16] and the peaks shown in figure 2b are found to be understood as σ transitions of the Balmer-α line at 350 G. The assignment of the peaks labeled in figure 2b are listed in table 1. It is noted that the apparent forbidden transition $2\,^2{\rm P}_{1/2,-1/2} - 3\,^2{\rm D}_{5/2,-3/2}$ in the group (7) in table 1 is due to mixing of the $3\,^2{\rm D}_{3/2,-3/2}$ wavefunction (approximately 5%) into $3\,^2{\rm D}_{5/2,-3/2}$ by the magnetic field. The unlabeled peaks shown in figure 2b are understood as cross-over signals.

Accordingly, it has been shown that a Zeeman-split spectrum of the Balmer-α line of atomic hydrogen is successfully measured by saturation spectroscopy with a resolution finer than the Doppler broadening. It is expected that the magnetic field strength (or the location of excitation in LHD) is derived from the saturation spectrum with Zeeman splitting, even in the case with varying magnetic field along the pathways of the laser beams [8]. It is noted that the saturation spectrum includes information on plasma parameters in addition to the magnetic field strength. The absorption coefficient for the probe beam ($\alpha^0_{\rm probe}$) represents the density of atomic hydrogen at the $n = 2$ state [3]. In addition, since the widths of the peak components in the saturation spectrum are basically determined by the natural and the Stark broadenings, it would be possible to evaluate the electron density and the electron temperature of the plasma from the profiles of the peak components [11–13]. For example, in the case of the high-density mode discharge, the peaks were broadened due to Stark broadening and were overlapped each other as shown in figure 3 (but the peaks (1), (2), (6), and (7) were observable). The analyses of the spectral distributions of the peak components will be reported elsewhere.

Table 1. Assignments of peaks shown in figures 2b and 3. Each energy level is denoted as $n^{2S+1}L_{J,M}$ where n is the principal quantum number, S, L, and J are the spin, orbital, and total angular momentum quantum numbers, respectively, and M is the magnetic quantum number. Lines having the transition probabilities larger than 10^6 s^{-1} are only listed.

Label	Wavelength (nm)	Transition probability (s^{-1})	Transition		
(1)	656.28643	7.640×10^6	$2^2\mathrm{P}_{3/2,1/2}$	–	$3^2\mathrm{D}_{3/2,3/2}$
	656.28612	8.365×10^6	$2^2\mathrm{P}_{3/2,3/2}$	–	$3^2\mathrm{D}_{5/2,1/2}$
	656.28608	9.649×10^6	$2^2\mathrm{P}_{3/2,-1/2}$	–	$3^2\mathrm{D}_{3/2,1/2}$
	656.28602	2.349×10^7	$2^2\mathrm{P}_{3/2,1/2}$	–	$3^2\mathrm{D}_{5/2,-1/2}$
	656.28594	4.315×10^7	$2^2\mathrm{P}_{3/2,-1/2}$	–	$3^2\mathrm{D}_{5/2,-3/2}$
	656.28590	6.459×10^7	$2^2\mathrm{P}_{3/2,-3/2}$	–	$3^2\mathrm{D}_{5/2,-5/2}$
	656.28571	6.724×10^6	$2^2\mathrm{P}_{3/2,-3/2}$	–	$3^2\mathrm{D}_{3/2,-1/2}$
(2)	656.28450	6.459×10^7	$2^2\mathrm{P}_{3/2,3/2}$	–	$3^2\mathrm{D}_{5/2,5/2}$
	656.28437	3.479×10^7	$2^2\mathrm{P}_{3/2,1/2}$	–	$3^2\mathrm{D}_{5/2,3/2}$
	656.28425	1.503×10^7	$2^2\mathrm{P}_{3/2,-1/2}$	–	$3^2\mathrm{D}_{5/2,1/2}$
	656.28414	4.041×10^6	$2^2\mathrm{P}_{3/2,-3/2}$	–	$3^2\mathrm{D}_{5/2,-1/2}$
(3)	656.27814	1.335×10^7	$2^2\mathrm{S}_{1/2,1/2}$	–	$3^2\mathrm{P}_{1/2,-1/2}$
(4)	656.27626	1.634×10^7	$2^2\mathrm{S}_{1/2,-1/2}$	–	$3^2\mathrm{P}_{1/2,1/2}$
	656.27614	1.443×10^6	$2^2\mathrm{P}_{1/2,1/2}$	–	$3^2\mathrm{S}_{1/2,-1/2}$
(5)	656.27426	1.359×10^6	$2^2\mathrm{P}_{1/2,-1/2}$	–	$3^2\mathrm{S}_{1/2,1/2}$
	656.27365	9.082×10^6	$2^2\mathrm{S}_{1/2,1/2}$	–	$3^2\mathrm{P}_{3/2,-1/2}$
	656.27321	2.243×10^7	$2^2\mathrm{S}_{1/2,-1/2}$	–	$3^2\mathrm{P}_{3/2,-3/2}$
(6)	656.27180	2.243×10^7	$2^2\mathrm{S}_{1/2,1/2}$	–	$3^2\mathrm{P}_{3/2,3/2}$
	656.27166	5.081×10^7	$2^2\mathrm{P}_{1/2,-1/2}$	–	$3^2\mathrm{D}_{3/2,-3/2}$
	656.27158	1.680×10^7	$2^2\mathrm{P}_{1/2,1/2}$	–	$3^2\mathrm{D}_{3/2,-1/2}$
	656.27131	6.092×10^6	$2^2\mathrm{S}_{1/2,-1/2}$	–	$3^2\mathrm{P}_{3/2,1/2}$
(7)	656.27054	1.785×10^7	$2^2\mathrm{P}_{1/2,-1/2}$	–	$3^2\mathrm{D}_{3/2,1/2}$
	656.27042	5.366×10^7	$2^2\mathrm{P}_{1/2,1/2}$	–	$3^2\mathrm{D}_{3/2,3/2}$
	656.27040	2.358×10^6	$2^2\mathrm{P}_{1/2,-1/2}$	–	$3^2\mathrm{D}_{5/2,-3/2}$

4.3 Evaluation of saturation parameter

According to equation (4.1), the amplitude of the saturation spectrum at $\omega = \omega_0$ is given by $\Delta\alpha_{\mathrm{probe}}/\alpha^0_{\mathrm{probe}} = 2S(1+S)/(1+\sqrt{1+S})^2$. On the other hand, the amplitude of the peak component shown in figures 5a and 6a is less than $\Delta\alpha_{\mathrm{probe}}/\alpha^0_{\mathrm{probe}} \simeq 0.1$, which corresponds to a saturation parameter of $S \simeq 0.2$. Hence the saturation parameter evaluated from the saturation spectrum observed in this experiment was less than ~ 0.2.

Another method to evaluate the saturation parameter experimentally is to observe the absorbance of the pump laser beam. Figure 7 shows the absorbance of the pump laser beam at a wavelength of 656.285 nm (at the origin of the relative frequency axis) as a function of the pump laser power. The solid curve shown in figure 7 represents a fitting between the experimental result

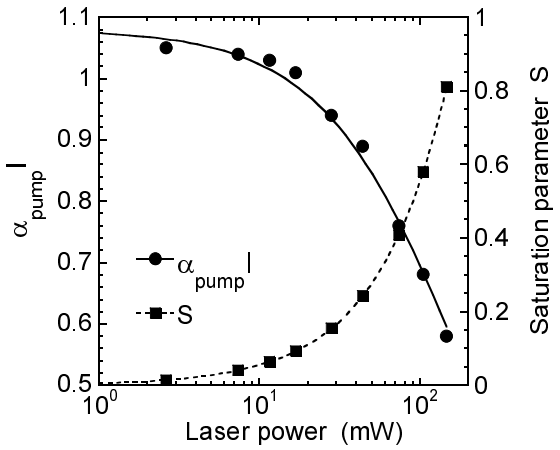

Figure 7. Relationship between the absorbance and the power of the pump laser beam. The solid curve shows the fitting between the experimental result and equation (4.3). The saturation parameter evaluated by the fitting is shown by the dashed curve.

and equation (4.3), indicating that the decrease in the absorbance agrees with the theory of saturation. The saturation parameter evaluated by the curve fitting is illustrated by the dashed curve in figure 7. Accordingly, the saturation parameter evaluated from the absorbance of the pump laser beam was $S \leq 0.8$. The saturation parameter of $S \leq 0.2$, which was evaluated from the amplitude of the saturation spectrum, may be underestimated, since equation (4.1) is accurate when $S \ll 1$. However, it is suggested that the amplitude of the saturation spectrum is smaller than that expected from the absorbance of the pump laser beam.

The saturation parameter is estimated theoretically using equation (4.2). The relaxation frequency R_2 is given by the transition probability of the Lyman-α line, the relaxation frequency R_3 is given by the sum of the transition probabilities of the Lyman-β and Balmer-α lines, B_{23} is given by the transition probability of the Balmer-α line, and ρ is evaluated from the pump laser intensity and the natural broadening width of the Balmer-α line. A theoretical saturation parameter of $S \sim 5$ was estimated by substituting the above values into equation (4.2). Accordingly, even when we consider the spatial distribution of the pump laser power due to absorption, the theoretical saturation parameter is larger than both the experimental saturation parameters evaluated from the amplitude of the saturation spectrum and the absorbance of the pump laser beam.

4.4 Characteristics of saturation spectrum

The experimental result shown in figure 5a is reasonable, since the saturation parameter is proportional to the pump laser power (equation (4.2)) and the amplitude of the saturation spectrum is roughly proportional to the saturation parameter (equation (4.1)). The saturation of the increase in $\Delta\alpha_{\mathrm{probe}}/\alpha^0_{\mathrm{probe}}$ in the high-power regime is attributed to the fact that equation (4.1) is accurate for $S \ll 1$. An experimental result that is difficult to be understood by the simple theory of saturation spectroscopy is the existence of the broadband offset component in the saturation spectrum, as shown in figures 2b and 3. As shown in figure 5b, the amplitude of the offset component had a similar variation to that of the peak component, when the pump laser power was varied. Since the

offset component makes the signal-to-noise ratio of the saturation spectrum smaller, it is important to know the mechanism for the broadband offset component.

The smaller experimental saturation parameter than theoretical one and the existence of the broadband offset component is explained by supposing the change in the velocity of atomic hydrogen due to collisions. This means the transport of atomic hydrogen in the velocity space. In other words, collisions transport a part of hydrogen atoms from the Lamb-dip region to the outside, resulting in the broadband offset component. The experimental result shown in figure 6 qualitatively supports the above hypothesis. The decrease in the peak amplitude with the gas pressure is explained by the increase in the collision frequency, and it in turn explains the increase in the amplitude of the broadband offset component.

In the above hypothesis, atomic hydrogen which changes the velocity is at an excited state with a principal quantum number of $n = 2$. Since the radiative lifetime of the $n = 2$ state is ~ 1.6 ns, direct collisions within the radiative lifetime are not expected. We speculate the following indirect collision process as the mechanism to explain the change in the velocity of atomic hydrogen. The excited ($n = 2$) and ground ($n = 1$) states of atomic hydrogen are strongly coupled via radiation and its trapping at the Lyman-α line. Therefore, if the velocity distribution function of the $n = 2$ state has a dip induced by the pump laser beam, it is expected that the velocity distribution function of the $n = 1$ state also has a dip, even though the depth of the dip of the $n = 1$ state is shallower than that of the $n = 2$ state. Since the lifetime of the $n = 1$ state is long enough, the dip in the velocity distribution function of the $n = 1$ state is filled up due to collisions. The change in the velocity distribution function of the $n = 1$ state due to collisions is reflected back to the velocity distribution function of the $n = 2$ state via radiation trapping. This is a possible mechanism which would explain the existence of the broadband offset component in the saturation spectrum and the smaller amplitude of the peak component than that expected by the theoretical saturation parameter. However, further investigations are necessary to obtain better understanding on the characteristics of the saturation spectrum.

5. Conclusions

We applied saturation spectroscopy to the Balmer-α line of atomic hydrogen with the intention of applying it to plasma diagnostics. We clearly observed fine-structure components with Zeeman splitting with Doppler-free spectral resolutions. We examined the amplitudes of the peak and offset components as functions of the pump laser power and the discharge gas pressure. The spectral characteristics have not been fully understood yet, and further investigations are necessary to apply saturation spectroscopy to diagnostics of LHD.

Acknowledgments

This work was supported by JSPS KAKENHI (21340174) and the NIFS Collaboration Research program (NIFS09KOAP022).

References

[1] S. Welzel, L. Gatilova, J. Röpcke, and A. Rousseau, *Time-resolved study of a pulsed dc discharge using quantum cascade laser absorption spectroscopy: NO and gas temperature kinetics, Plasma Sources Sci. Technol.* **16** (2007) 822.

[2] J. Röpcke, G. Lombardi, A. Rousseau, and P. B. Davies, *Application of mid-infrared tunable diode laser absorption spectroscopy to plasma diagnostics: a review, Plasma Sources Sci. Technol.* **15** (2006) S148.

[3] M. Aramaki, Y. Okumura, M. Goto, S. Muto, S. Morita, and K. Sasaki, *Measurements of gas temperature in high-density helicon-wave H_2 plasmas by diode laser absorption spectroscopy, Jpn. J. Appl. Phys.* **44** (2005) 6759.

[4] A. Rousseau, E. Teboul, and N. Sadeghi, *Time-resolved gas temperature measurements by laser absorption in a pulsed microwave hydrogen discharge, Plasma Sources Sci. Technol.* **13** (2004) 166.

[5] H. Scheibner, St. Franke, Samir Solyman, J. F. Behnke, C. Wilke, and A. Dinklage, *Laser absorption spectroscopy with a blue diode laser in an aluminum hollow cathode discharge, Rev. Sci. Instrum.* **73** (2002) 378.

[6] M. Hiramatsu, M. Sakakibara, M. Mushiga, and T. Goto, *Measurement of the density and translational temperature of Si($3p^2$ $^1D_2$) atoms in RF silane plasma using UV laser absorption spectroscopy, Meas. Sci. Technol.* **2** (1991) 1017.

[7] M. Goto, K. Sawada, and T. Fujimoto, *Relations between the ionization or recombination flux and the emission radiation for hydrogen and helium in plasma, Phys. Plasmas* **9** (2002) 4316.

[8] M. Goto and S. Morita, *Determination of the line emission locations in a large helical device on the basis of the Zeeman effect, Phys. Rev. E* **65** (2002) 026401.

[9] A. Iwamae, M. Hayakawa, M. Atake, T. Fujimoto, M. Goto, and S. Morita, *Polarization resolved H_α spectra from the large helical device: Emission location, temperature, and inward flux of neutral hydrogen, Phys. Plasmas* **12** (2005) 042501.

[10] B. W. Petley, K. Morris, and R. E. Shawyer, *A saturated absorption spectroscopy measurement of the Rydberg constant, J. Phys. B: Atom. Molec. Phys.* **13** (1980) 3099.

[11] E. W. Weber, *Shift and broadening of resolved hydrogen Balmer-α fine-structure lines in helium, Phys. Rev. A* **20** (1979) 2278.

[12] E.W. Weber and H.J. Humpert, *Plasma shift and broadening of single hydrogen Balmer-α fine-structure lines, Phys. Lett.* **83** (1981) 386.

[13] E. W. Weber, R. Frankenberger, and M. Schilling, *Nonlinear plasma spectroscopy of the hydrogen Balmer-α line, Appl. Phys. B* **32** (1983) 63.

[14] M. Aramaki, K. Kato, M. Goto, S. Muto, S. Morita, and K. Sasaki, *Development of a compact divertor simulator excited by helicon-wave discharge, Jpn. J. Appl. Phys.* **43** (2004) 1164.

[15] W. Demtröder, *Laser Spectroscopy, 4th edition*, Springer-Verlag, Berlin Heidelberg 2008.

[16] M. Goto, Chapter 2 in *Plasma Polarization Spectroscopy* edited by T. Fujimoto and A. Iwamae, Springer-Verlag, Berlin Heidelberg 2008.